03

Photoelectric properties of structures with GeSiSn|Ge multiple quantum wells and relaxed GeSiSn layers

© V.A. Timofeev[1], I.V. Skvortsov[1], V.I. Mashanov[1], A.A. Bloshkin[1], V.V. Kirienko[1], I.D. Loshkarev[1], T.M. Zalyalov[1,2], T.V. Perevalov[1], D.R. Islamov[1,2]

[1] Rzhanov Institute of Semiconductor Physics, Siberian Branch, Russian Academy of Sciences, Novosibirsk, Russia
[2] Novosibirsk State University, Novosibirsk, Russia

E-mail: damir@isp.nsc.ru

Received October 4, 2024
Revised October 13, 2024
Accepted October 13, 2024

The photoelectric properties of p-i-n photodiodes including GeSiSn|Ge multiple quantum wells (MQWs) and relaxed GeSiSn layers on a Ge(1 0 0) substrate have been studied. Based on current-voltage characteristic measurements, it is shown that the lowest density of the dark current of p-i-n photodiodes with a reverse bias of 1 V reaches a value of 0.7 mA/cm^2. The cut-off wavelength for both diodes with MQWs and relaxed layers is about 2 μm ($\sim$ 0.6 eV).

Keywords: molecular beam epitaxy, multiple quantum wells, relaxed layer, diffraction reflection curve, photodiode, photocurrent, dark current, sensitivity limit.

DOI: 10.61011/PSS.2024.11.60085.255

1. Introduction

The ever-increasing requirements for silicon microelectronics devices, such as miniaturization, increased performance, and improved energy efficiency, are driving the creation of new approaches to manufacturing electronic components. The embedding of high-bandwidth optical communication between the elements of integrated circuits is one of such approaches. The absence of photon interaction is the key advantage of optical data transmission which opens up the possibility of simultaneous transmission of several signals over a single communication channel. The wavelength range from 1.1 to 3 μm [1] is the most suitable for building optoelectronic integrated circuits operating at room temperature. Photonics devices based on GeSiSn triple compositions are the most promising in this regard [2]. The indisputable advantage of this material class is compatibility with the technological processes of modern silicon microelectronics. Varying the composition of GeSiSn allows not only to change the band gap in a wide range, but also to obtain direct-band-gap semiconductors [3–5]. The controlled management of the GeSiSn electronic structure is critically important for manufacturing efficient light-emitting and detecting devices in the short-wavelength infrared (IR) range.

There are a number of problems in the path of forming the element base of photonics based on GeSiSn. First of all, these are high mechanical stresses and a high density of penetrating dislocations in the deposited layers due to a significant mismatch of the parameters of the Sn, Si, and Ge lattices. Secondly, these are the effects of tin segregation and precipitation due to its low equilibrium solubility in Ge ($< 1\%$) and Si ($< 0.1\%$) [6,7]. Nonequilibrium growth methods such as low-temperature molecular beam epitaxy (MBE) and vapor-phase epitaxy are used to overcome low solubility [8]. Finally, a fundamentally important task is to optimize the resulting structures in terms of heterocomposition, composition, and thickness of GeSiSn layers. The solution to this problem is at the forefront of studies of structures based on GeSiSn.

Intensive studies are currently underway in this area, and a number of significant results have already been obtained. The p-i-n diode design is most often used as the photodetecting device structure in studies of photodiodes. This type of photodetector is characterized by high sensitivity and high performance at low operating voltage. The electro-optical properties of GeSiSn-based p-i-n diodes with two and four quantum wells (QW) are compared [9]. It was shown that the dark current density value in a structure with two QW is less than in one with four QW, but has a high value of $\sim$ 10 A/cm^2 at a reverse voltage of 1 V. The sensitivity of the photodetector with four QW is several times higher, but the photoresponse was limited to a wavelength of about 1.7 μm for both diodes. The characteristics of GeSiSn-based p-i-n structures with different compositions and materials of electrical contacts were studied in another paper [10]. It has been shown that the lowest dark current density is achieved in case of usage of a Ni-Al contact to a GeSiSn layer containing Sn 9.5%.

In this paper, two types of p-i-n structures are studied, including GeSiSn multiple quantum wells (MQW) and relaxed GeSiSn layers on a Ge(1 0 0) substrate. The

Growth parameters of samples of p-i-n structures. ρ is degree of the GeSiSn layer relaxation

Sample	Ge, %	Si, %	Sn, %	d_{GSS}, nm	Type of structure	ρ, %
Q1, Q2	3	85	12	1	MQW	0
Q3, Q4	14	76	10	200	one layer GeSiSn	92
Q5, Q6	12	78	10	200		91
Q7, Q8	30	60	10	200	top layer GeSiSn	72
					bottom layer GeSiSn	2.5

structural and photoelectric properties of photodiodes are studied.

2. Experiment

The studied p-i-n structures were grown by low-temperature MBE on n^+-Ge(1 0 0) substrate. The active region of the structures included either GeSiSn|Ge MQW or relaxed GeSiSn layers with a thickness of $d_{\mathrm{GSS}} = 200$ nm (see table). GeSiSn|Ge MQW consisted of 10 GeSiSn layers with a thickness of $d_{\mathrm{GSS}} = 1$ nm, separated by Ge barrier layers with a thickness of 7 nm. The MBE growth chamber has an electron beam evaporator (EBE) for Si and Ge, as well as effusion cells for Sn and B. The B source was used to form p^+-Ge layers. The use of Ge EBE made it possible to grow Ge layers at a rate of up to 0.2 nm/s (without loss of the quality of the applied films), whereas the growth rate of Ge layers in case of deposition from the effusion cell did not exceed 0.02 nm/s. Increasing the Ge evaporation rate significantly reduced the growth time of the whole p-i-n structure. The i-Ge buffer layer thickness in all structures was 200 nm, and the thickness of the i-Ge layer grown on top of the GeSiSn layers was 100 nm. The temperature of i-Ge upper layer varied in the range of 150−300°C. The heavily-doped p^+-Ge layer reached a thickness of 200 nm. GeSiSn layers were deposited at a temperature of 150°C in all samples. The compositions of the GeSiSn layers and the structural parameters of the obtained samples are described in the table. The morphology of the surface was controlled using reflection high-energy electron diffraction (RHEED) during the growth process. The stress state and composition of GeSiSn layers in p-i-n structures were studied by X-ray diffractometry. A two-crystal X-ray diffractometer DSO-1T with Ge(0 0 4) monochromator crystal using $\mathrm{Cu}_{K\alpha 1}$ radiation was used to measure the diffraction reflection curves.

The photodiodes were formed as a circular mesa with a diameter of 700 μm with an annular upper contact (Figure 1). Standard technological processes were used in the manufacture: optical lithography, plasma etching, and metal deposition in vacuum. Plasma chemical etching of the mesa was carried out in Plasmalab System 80 system using CF4 + Ar gas mixture through a photoresist mask. The structure was etched to the full depth down to the Ge substrate. Thin gold metal films with a thickness of 50−100 nm were used to form electrodes for doped Ge layers. A Ti sublayer with a thickness of 5 nm was deposited before the Au layer deposition to increase the adhesion of Au to the surface. The plate with the finished photodiodes was cut into chips, which were mounted on ceramic pads to measure current-voltage and photovoltaic characteristics. The thin silver wires used as conductors were connected to the contact pads of the diodes by cold welding. The dark current of the diodes was monitored at room temperature using Keithley 2450 source-measure unit.

The spectral characteristics of p-i-n photodiodes based on Ge|GeSiSn|Ge heterostructures were measured using Bruker Vertex-70 IR-Fourier spectrometer. The sample was placed in vacuum cryostat Janis-VPF100 equipped with a Lakeshore Model 325 controller for the temperature stabilization. Liquid nitrogen was used for cooling. The structures were illuminated by near-infrared radiation from a halogen lamp to study the photocurrent. The photocurrent was measured using a low-noise SR570 preamplifier from Stanford Research Systems. The photocurrent spectra obtained using the Fourier transform were normalized to the emission spectrum of the halogen lamp.

3. Results and discussion

The structural and photovoltaic properties of a series of p-i-n structures, including GeSiSn|Ge MQW and relaxed GeSiSn layers, were studied. The experimental and calculated (0 0 4) diffraction reflection curves are shown in Figure 2, *a* for the sample Q1, which includes GeSiSn|Ge MQW. The diffraction reflection curves contain a Ge substrate peak, a zero peak from a periodic structure with MQW, as well as a superposition of thickness oscillations with a short period. The position of the zero satellite corresponds to the average composition of the MQW structure. The estimated of the GeSiSn layer compositions are listed in the table. The shape of the experimental curve is in good agreement with the modeling results. This confirms the elastic stress state of the GeSiSn layers. Their lattice parameter in the unstressed state is 5.578 Å. The mismatch between the GeSiSn and Ge lattice parameters is 1.4%.

The intensity distribution in the reciprocal space around the Ge(2 2 4) node of the reciprocal lattice was mapped for samples of Q3–Q7 (Figure 2, *a–d*). A slit in front of the detector with an angular aperture of 70 arc sec was used as an analyzer. The reciprocal space maps in Figure 2, *b* (sample Q3) and Figure 2, *c* (sample Q5) contain two peaks: the Ge substrate peak and the GeSiSn peak (relaxation $\rho = 92$ and 91%, the lattice parameters in the unstressed state are 5.583 and 5.579 Å respectively). Figure 2, *b* shows

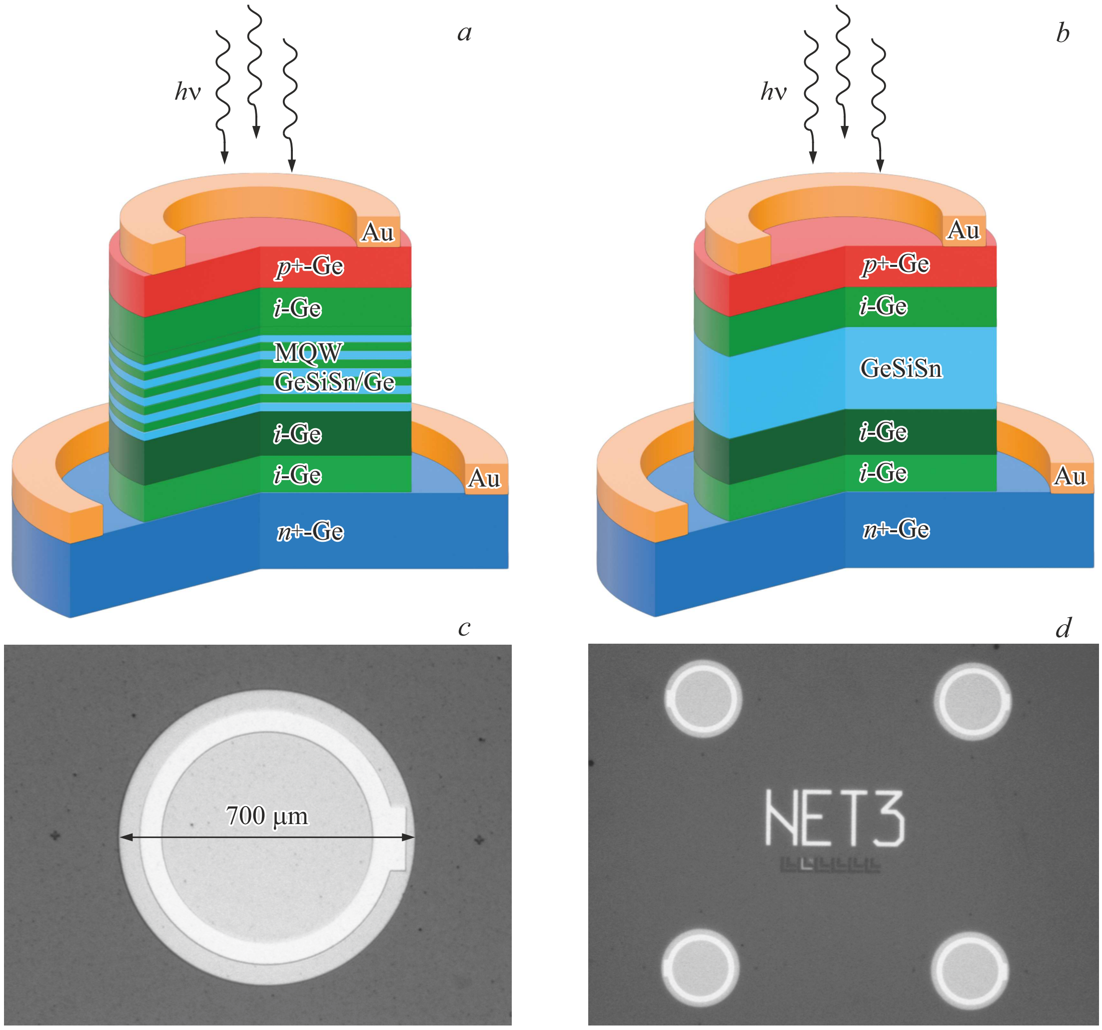

Figure 1. (Color Online) Schematic representation of p-i-n photodiodes containing *a*) GeSiSn|Ge MQW and *b*) relaxed GeSiSn layer. *c*) Optical image of a p-i-n photodiode with a mesa diameter of 700 μm. *d*) An optical image of a chip with multiple diodes.

the intensity distribution from the substrate node towards an increase of the lattice parameter up to 5.699 Å with stress relaxation 25%. This can be explained by the diffusion of tin into the upper Ge layers due to the increased temperature of their growth up to 300°C. The Ge(2 2 4) substrate node is located in the zero position of the reciprocal space map for sample Q7 (Figure 2, *d*). A node of an almost pseudomorphic GeSiSn film (degree of relaxation is 2.5%) with a lattice parameter of 5.609 Å is located vertically above it. In addition, there is another film node nearby with the parameter 5.612 Å and the degree of relaxation 72%. Thus, it can be assumed that two GeSiSn layers of different composition were formed: the lower GeSiSn layer, coherently conjugated with the Ge substrate, and the upper one is partially relaxed GeSiSn layer. The upper Ge layers, which form the Ge(2 2 4) node near the substrate node, are pseudomorphically conjugated with the upper partially relaxed GeSiSn layer. The upper Ge layer is in a compressed state relative to the bulk Ge and is deformed by 0.42%.

The current-voltage characteristics (IV) of Q1–Q8 photodiode series, measured at room temperature, are shown in Figure 3. Diode IV curves are observed for all samples. Q7 and Q8 samples have maximum rectification coefficients (up to $4 \cdot 10^4$) among the entire series of photodiodes and a minimum dark current density of about 0.7 mA/cm^2 with reverse bias 1 V. In addition, the values of the imperfection factor *n*were determined (Figure 3) [11]. The best values of n, close to one, were obtained for samples Q7 and Q8. This may be due to the low concentration of deep centers in the i-region of the p-i-n photodiodes. For photodiodes with high *n* values, the presence of deep levels can lead to an increase of tunneling and recombination leakage currents, which provide an additional contribution to the dark current of the photodiode. The concentration of deep centers is determined by the temperature of the upper Ge layers in the p-i-n photodiode. An increase of the substrate temperature increases the diffusion of tin from the GeSiSn layers and leads to an increase of the vacancy complex density, which

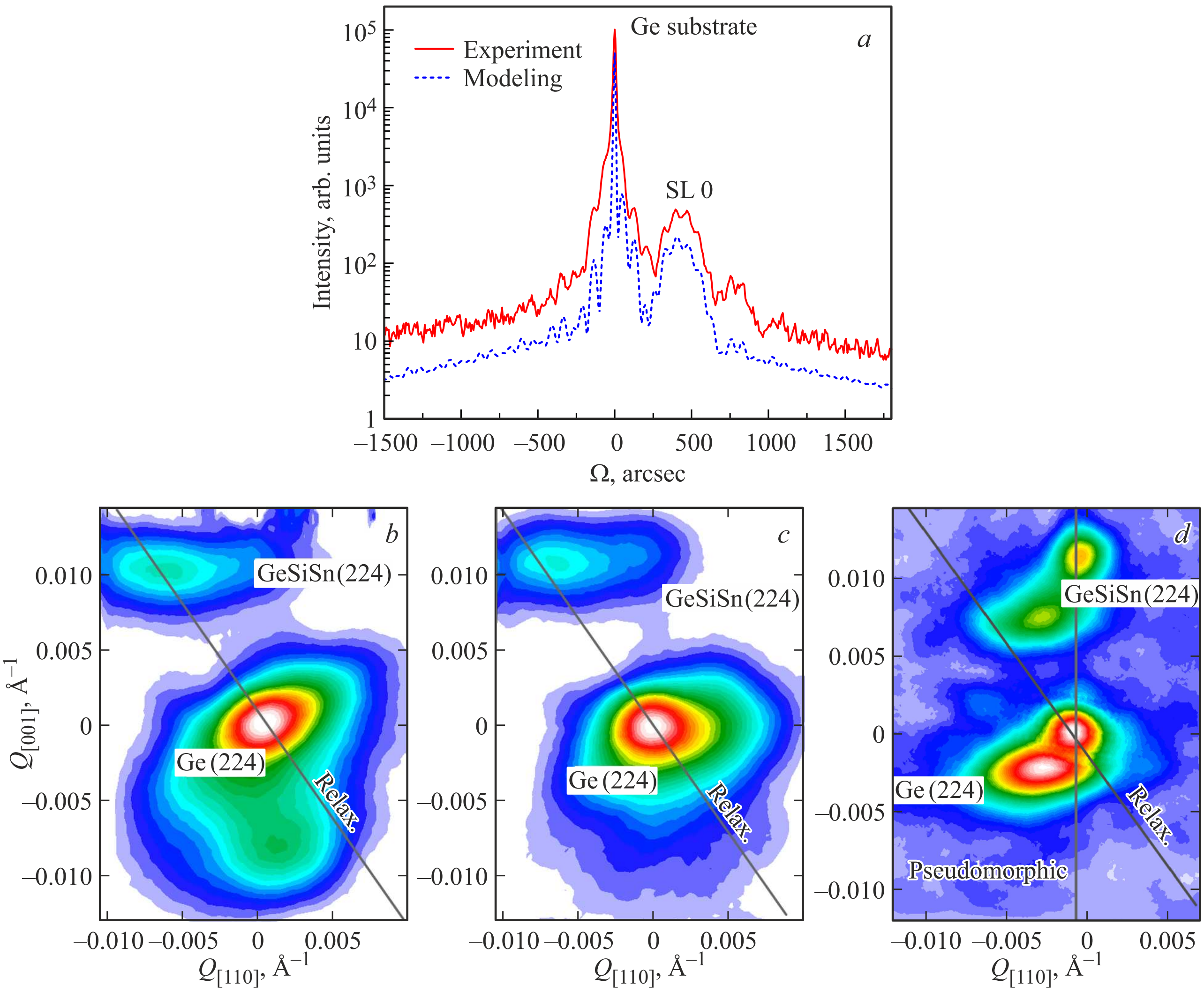

Figure 2. (Color Online) *a*) (0 0 4) diffraction reflection curves for p-i-n structures including the GeSiSn|Ge MQW. Maps of the reciprocal space near the (2 2 4) reflex for a series of samples *b*) Q3, *c*) Q5 and *d*) Q7 that include relaxed GeSiSn layers. Lines of complete relaxation and a line of pseudomorphic conjugation of films are shown in the maps.

can act as deep centers [12,13]. Therefore, the best device characteristics are observed in samples Q7 and Q8 obtained at the lowest growth temperature of the upper Ge layers.

The spectra of the photocurrent of p-i-n photodiodes, including the GeSiSn|Ge MQW and relaxed GeSiSn layers, were analyzed (Figure 4, *a–d*). The spectral dependences of the photocurrent were measured in the temperature range of 77–300 K. An increase of the photocurrent signal is observed for all samples with an increase of the temperature, which may be explained by an increase of the number of phonons involved in interband recombination processes. An increase of the sample temperature causes a shift of the long-wavelength sensitivity boundary towards longer wavelengths due to a decrease in the band gap. Figure 4, *e* shows the temperature dependences of the long-wavelength sensitivity boundary. The theoretical dependence of the band gap width for pure germanium is shown for comparison (Figure 4, *e*). One can see that the boundary absorption energy in the GeSiSn layers for all samples is significantly lower than the theoretical limit achievable in germanium photodetectors. The values of the long-wavelength sensitivity limit at room temperature for a series of photodiodes range from 2.01 to 2.14 μm. The spectral dependences of the photocurrent measured at room temperature and normalized to the values of the photocurrent at a wavelength of 1.55 μm are shown in Figure 4, *f*. The highest photocurrent signal is observed in the whole sensitivity range for the Q7 photodiode. The largest difference in the intensity of the photoresponse signals of the Q7 sample in comparison with other samples is 3–4 times in the wavelength range of 1.8–1.9 μm. Thus, the use of GeSiSn layers allows moving towards longer operating wavelengths compared to Ge layer-based photodetectors.

The energies of possible optical transitions in GeSiSn|Ge heterostructures were estimated by constructing band dia-

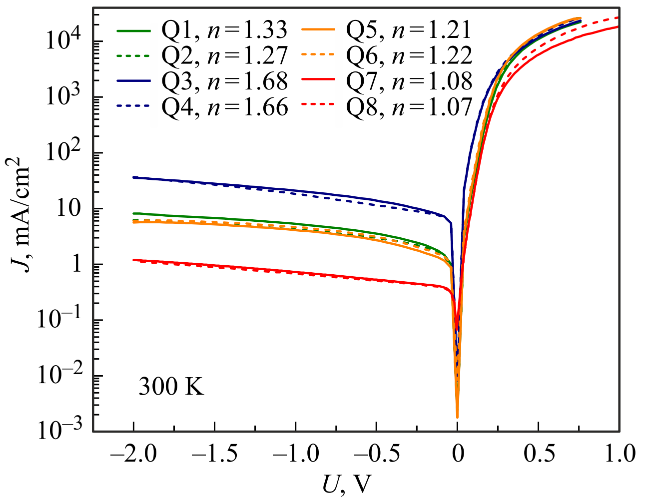

Figure 3. (Color Online) Current-voltage characteristics of p-i-n photodiodes: Q1 and Q2 are based on the GeSiSn|Ge MQW; Q3–Q8 are based on the relaxed GeSiSn layers.

grams using the approach described in Ref. [15]. The size of the gap in the valence bands between Ge and GeSiSn was determined in a linear approximation for compositions:

$$\Delta E_v\,(\mathrm{Ge}_{1-x-y}\mathrm{Si}_x\mathrm{Sn}_y) = -x\cdot\Delta E_v^{\mathrm{GeSi}} + y\cdot\Delta E_v^{\mathrm{GeSn}},$$

where $\Delta E_v^{\mathrm{GeSi}} = 0.54\,\mathrm{eV}$ and $\Delta E_v^{\mathrm{GeSn}} = 0.69\,\mathrm{eV}$ are the breaks of valence bands at the Ge–Si and Sn–Ge heterojunctions, respectively [16,17]. The value $E_v(\mathrm{Ge})$ was taken as the zero energy level. The positions of the subbands of heavy (E_{HH}) and light (E_{LH}) holes were determined based on the following expressions:

$$E_{\mathrm{HH}} = E_{\mathrm{LH}} = \Delta E_v + \Delta_0/3,$$

$$\Delta_0 = 0.295(1-x-y) + 0.043x + 0.8y,$$

where Δ_0 is the spin-orbit splitting energy in GeSiSn [17]. The positions of the valleys of the conduction band were calculated in the quadratic approximation:

$$E_g^{\xi}(\mathrm{Ge}_{1-x-y}\mathrm{Si}_x\mathrm{Sn}_y) = (1-x-y)E_g^{\xi}(\mathrm{Ge}) + xE_g^{\xi}(\mathrm{Si}) + yE^{\xi}(\mathrm{Sn}) - x(1-x-y)b^{\xi}_{\mathrm{SiGe}} - y(1-x-y)b^{\xi}_{\mathrm{GeSn}} - xyb^{\xi}_{\mathrm{SiSn}}.$$

Here $E_g^{\xi}(\mathrm{Ge})$, $E_g^{\xi}(\mathrm{Si})$ and $Eg^{\xi}(\mathrm{Sn})$ are the values of the band gap Ge, Si and Sn; b^{ξ}_{SiGe}, b^{ξ}_{GeSn} and b^{ξ}_{SiSn} are the bowing parameters, which are entered to account for deviations from the linear law [17]. The index ξ corresponds to a specific valley. Then, the displacement of the position of the subbands under the impact of deformations in the GeSiSn layers was determined. For this purpose the values of deformations were found in the plane of the layer ($\varepsilon_{\parallel}$) and in the direction perpendicular to the GeSiSn layer ($\varepsilon_{\perp}$):

$$\varepsilon_{\parallel} = \frac{a_{\mathrm{Ge}} - a_{\mathrm{GeSiSn}}}{a_{\mathrm{Ge}}}, \quad \varepsilon_{\perp} = -2\frac{C_{12}}{C_{11}}\varepsilon_{\parallel},$$

$$a_{\mathrm{GeSiSn}} = (1-x-y)a_{\mathrm{Ge}} + xa_{\mathrm{Si}} + ya_{\mathrm{Sn}} + x(1-x)b'_{\mathrm{SiGe}} + y(1-y)b'_{\mathrm{SnGe}},$$

where C_{ij} is the elastic modulus [18], a_{X} is the material lattice parameter X; b'_{SiGe} and b'_{SnGe} are bowing parameters [17]. Then, the positions of the subbands of the conduction band and the valence band of the elastically stressed GeSiSn layers were found using the strain potential constants given in Ref. [18]. Figure 5 shows a band diagram for Ge|Ge$_{0.03}$Si$_{0.85}$Sn$_{0.12}$|Ge heterostructure. It can be seen from the constructed band diagram that the minimum of the conduction band in the GeSiSn layer is located in the Γ valley. Since the studied structures (samples Q1 and Q2) include Ge|GeSiSn|Ge quantum wells with a width of 1 nm, the value of the basic level of dimensional quantization of an electron in a quantum well was calculated. The one-dimensional stationary Schrodinger equation was solved for this purpose.

The effective mass m^*_{GeSiSn} in the GeSiSn layer along the growth direction was determined in a linear approximation:

$$m^*_{\mathrm{GeSiSn}} = (1-x-y)m^*_{\mathrm{Ge}} + xm^*_{\mathrm{Si}} + ym^*_{\mathrm{Sn}},$$

where $m^*\mathrm{Ge} = 0.038m_0$, $m^*\mathrm{Si} = 0.188m_0$, and $m^*\mathrm{Sn} = -0.058m_0$ are the effective electron masses in Γ-valleys along the growth direction for germanium, silicon, and tin, respectively [19]. Here m_0 is the mass of the free electron. As a result of the calculations, it was found that the lowest energy corresponds to the interband optical transition of an electron between the level of dimensional quantization in the Γ-valley of the GeSiSn layer and the ceiling of the Ge valence band (Figure 5). The obtained value of the interband optical transition was 0.6 eV. This value is in good agreement with the value of the long-wavelength sensitivity limit of the p-i-n photodiode based on the GeSiSn|Ge MQW (sample Q1). A similar approach was used to estimate the band gap of thick relaxed GeSiSn layers, but without taking into account dimensional quantization. Deformations in the relaxed layer ($\varepsilon_{\parallel}^{\mathrm{relax}}$ and $\varepsilon_{\perp}^{\mathrm{relax}}$) were determined using the expressions

$$\varepsilon_{\parallel}^{\mathrm{relax}} = \frac{a^{\parallel}_{\mathrm{GeSiSn}} - a_{\mathrm{GeSiSn}}}{a^{\parallel}_{\mathrm{GeSiSn}}},$$

$$\varepsilon_{\perp}^{\mathrm{relax}} = -2\frac{C_{12}}{C_{11}}\varepsilon_{\parallel}^{\mathrm{relax}},$$

where $a^{\parallel}_{\mathrm{GeSiSn}}$ is the experimental value of the lattice parameter in the plane of the relaxed layer. The band gap of the relaxed GeSiSn layers corresponds to the energy difference between the minimum of the conduction band in the Γ-valley and the maximum of the valence band, which is located in the subband of light holes. The calculated values of the band gap of the GeSiSn layers for samples

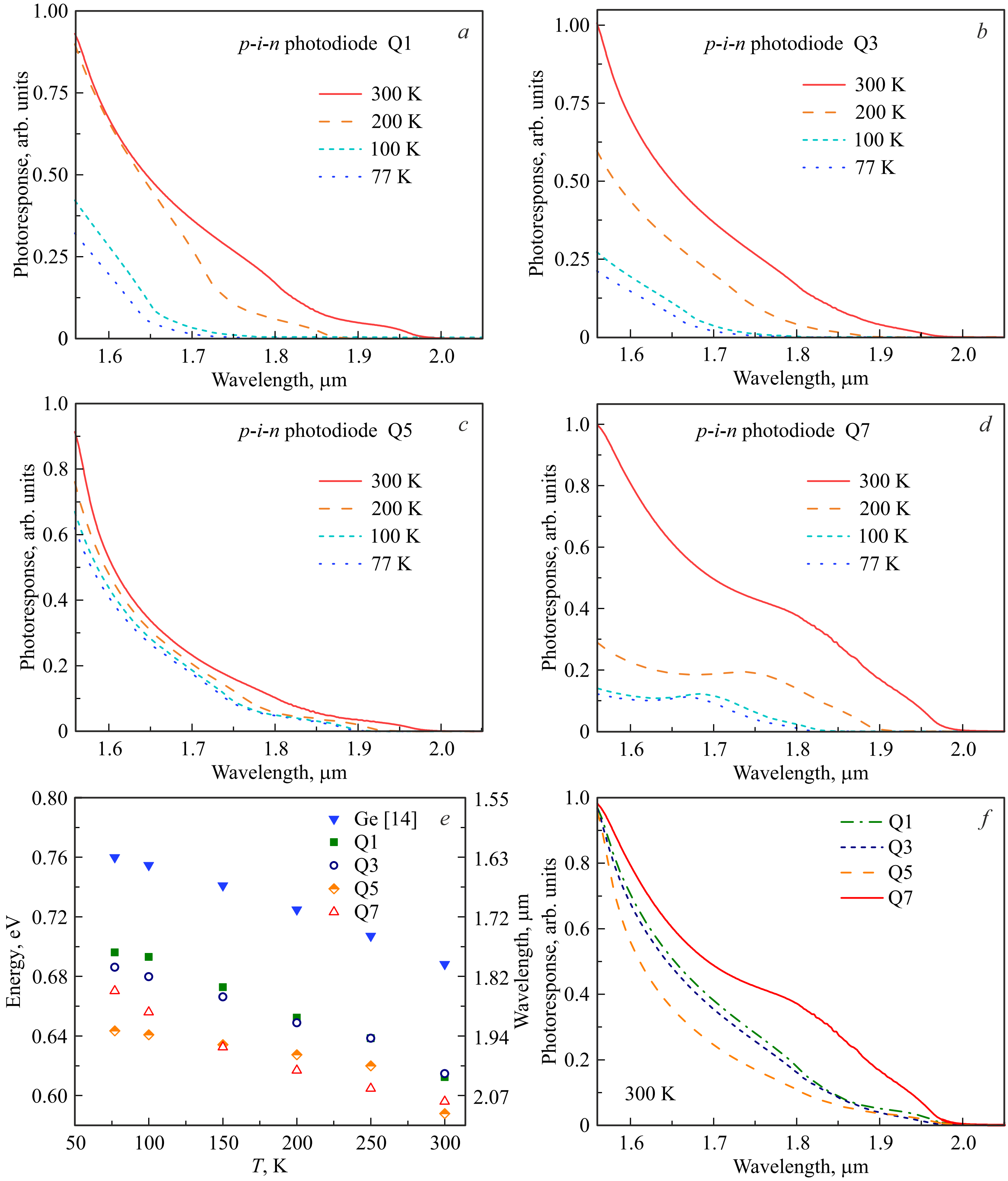

Figure 4. (Color Online) Photocurrent spectra of p-i-n photodiodes: based on *a*) GeSiSn|Ge MQW and *b*), *c*) and *d*) — based on relaxed GeSiSn layers. *e*) Temperature dependences of the long-wavelength sensitivity limits for samples Q1, Q3, Q5, and Q7 in comparison with the values of the Ge band gap taken from Ref. [14]. *f*) Photocurrent spectra of p-i-n photodiodes, normalized to photocurrent values at a wavelength of 1.55 μm.

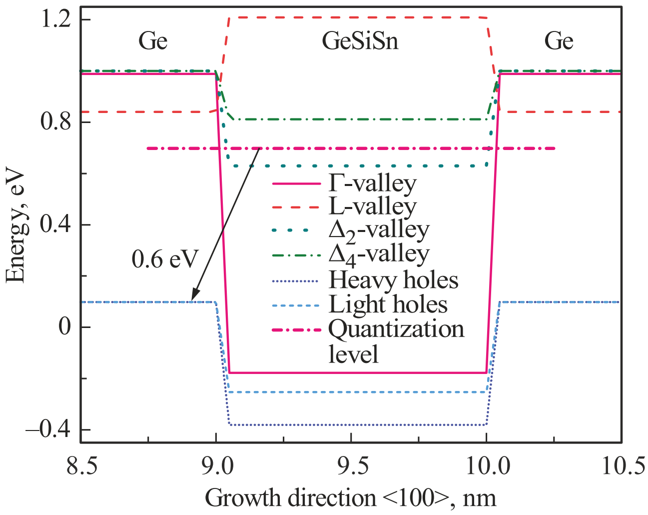

Figure 5. (Color Online) Band diagram for Ge|$Ge_{0.03}Si_{0.85}Sn_{0.12}$|Ge quantum well with a width of 1 nm.

Q3, Q5, and Q7 are approximately 0.6 eV, which is also in good agreement with the values of the long-wavelength sensitivity limit of p-i-n photodiodes comprising relaxed GeSiSn layers.

4. Conclusion

The structural and electrophysical properties of a series of p-i-n photodiodes based on the GeSiSn|Ge MQW and relaxed GeSiSn have been studied. The growth parameters of p-i-n structures are optimized to achieve the best diode characteristics. The lowest dark current density of p-i-n photodiodes was 0.7 mA/cm^2 at the inverse offset of 1 V. The long-wavelength limit of sensitivity for both MQW and relaxed layer diodes is about 2 μm ($\sim$ 0.6 eV). A band diagram is calculated for the Ge|GeSiSn|Ge heterostructure with an elastically stressed GeSiSn layer. The band gap width for relaxed GeSiSn layers is estimated. The results obtained demonstrate the prospects of using photodiodes based on GeSiSn|Ge heterostructures in the short-wavelength infrared range.

Funding

The work was performed within the framework of the state assignment of the Ministry of Education and Science of the Russian Federation for the Rzhanov Institute of Semiconductor Physics of the Siberian Branch of the Russian Academy of Sciences No. FWGW-2024-0001 „Physical and technological foundations of creating heterostructures based on group IV elements compatible with modern silicon technology for photonics devices“.

Conflict of interest

The authors declare the absence of conflicts of interest.

References

[1] R. Soref. In: 2016 IEEE Photonics Society Summer Topical Meeting Series (SUM), 100. Newport Beach, California, USA (2016).
[2] R. Soref. Phil. Trans. R. Soc. A **372**, *2012*, 20130113 (2014).
[3] R.A. Soref, C.H. Perry. J. Appl. Phys. **69**, *1*, 539 (1991).
[4] M. Bauer, C. Ritter, P.A. Crozier, J. Ren, J. Menendez, G. Wolf, J. Kouvetakis. Appl. Phys. Lett. **83**, *11*, 2163 (2003).
[5] P. Moontragoon, Z. Ikonić, P. Harrison. Semicond. Sci. Technol. **22**, *7*, 742 (2007).
[6] R. Ragan, K.S. Min, H.A. Atwater. Mater. Sci. Eng. B **87**, *3*, 204 (2001).
[7] T. Tsukamoto, N. Hirose, A. Kasamatsu, T. Mimura, T. Matsui, Y. Suda. Appl. Phys. Lett. **106**, *5*, 052103 (2015).
[8] S. Wirths, D. Buca, S. Mantl. Prog. Cryst. Growth Charact. Mater. **62**, *1*, 1 (2016).
[9] I.A. Fischer, T. Wendav, L. Augel, S. Jitpakdeebodin, F. Oliveira, A.Benedetti, S. Stefanov, S. Chiussi, G. Capellini, K. Busch, J. Schulze. Opt. Express. **23**, *19*, 25048 (2015).
[10] C.J. Clausen, I.A. Fischer, D. Weisshaupt, F. Baerwolf, B. Tillack, G. Colston, M. Myronov, M. Oehme, J. Schulze. Semicond. Sci. Technol. **33**, *12*, 124017 (2018).
[11] S.M. Sze. Physics of Semiconductor Devices. Wiley-Interscience (1969).
[12] V. Timofeev, I. Skvortsov, V. Mashanov, A. Nikiforov, D. Kolyada, D. Firsov, O. Komkov, S. Samadov, A. Sidorin, O. Orlov. J. Vac. Sci. Technol. B **42**, *3*, 030601 (2024).
[13] S. Zaima, O. Nakatsuka, N. Taoka, M. Kurosawa, W. Takeuchi, M. Sakashita. Sci. Technol. Adv. Mater. **16**, *4*, 043502 (2015).
[14] P. Geng, W. Li, X. Zhang, X. Zhang, Y. Deng, H. Kou. J. Phys. D: Appl. Phys. **50**, *40*, 40LT02 (2017).
[15] C.G. Van de Walle. Phys. Rev. B **39**, *3*, 1871 (1989).
[16] M. El Kurdi, S. Sauvage, G. Fishman, P. Boucaud. Phys. Rev. B **73**, *19*, 195327 (2006).
[17] P. Moontragoon, P. Pengpit, T. Burinprakhon, S. Maensiri, N. Vukmirovic, Z. Ikonic, P. Harrison. J. Non-Cryst. Solids. **358**, *17*, 2096 (2012).
[18] A. Attiaoui, O. Moutanabbir. J. Appl. Phys. **116**, *6*, 063712 (2014).
[19] Z. Chen, Z. Ikonic, D. Indjin, R.W. Kelsall. J. Appl. Phys. **129**, *12*, 123102 (2021).

Translated by A.Akhtyamov